pubs.acs.org/Biomac

Article

Engineering a Plant Viral Coat Protein for *In Vitro* Hybrid Self-Assembly of CO_2-Capturing Catalytic Nanofilaments

Suhan Wi, In Seong Hwang, and Byung Hoon Jo*

Cite This: *Biomacromolecules* 2020, 21, 3847−3856

Read Online

ACCESS | Metrics & More | Article Recommendations | Supporting Information

ABSTRACT: Plant virus-based nanoparticles are used as self-assembled protein scaffolds for the construction of enzyme nanocarriers. To date, one-pot production and coupling of both enzymes and scaffolds by genetic conjugation have been demonstrated only in plants. Herein, we report bacterial production and *in vitro* self-assembly of nanofilaments for CO_2 capture. Filamentous virus-like particles (VLPs) were successfully formed by genetically fusing carbonic anhydrase from *Hydrogenovibrio marinus* (*hm*CA) to the N terminus of the coat protein (CP_{PVY}) of potato virus Y with a flexible linker. The instability of VLPs against proteolytic degradation was circumvented by the periplasmic export of the fusion protein. The truncated form of CP_{PVY} coexpressed by internal translation was crucial for the successful formation of long filamentous VLPs by alleviating steric hindrance *via* hybrid assembly. The fast and economic bottom-up fabrication of highly active nanobiocatalyst allows the nanofilaments to be efficiently used and recovered in potential biocatalytic and biosensor systems.

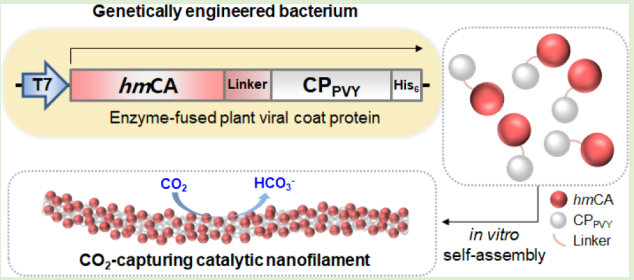

INTRODUCTION

Carbonic anhydrase (CA, EC 4.2.1.1) is a zinc-containing metalloenzyme that catalyzes the hydration of carbon dioxide (CO_2) as follows: $CO_2 + H_2O \leftrightarrow HCO_3^- + H^+$.[1] Owing to the diffusion-limited kinetics, with a k_{cat} of up to 4.4×10^6 s^{-1} and the green nature of biobased catalysts,[2] CA has been considered a promising alternative to its physical or chemical counterparts for the mitigation of greenhouse gas emissions.[3,4] In this bioinspired approach, CA can be employed not only for CO_2 absorption but also for CO_2 utilization processes such as mineral carbonation, electrochemical CO_2 reduction to formate, or photoautotrophic microbial cultivation.[5−10] In addition, CA has been applied to the development of biosensors for the detection of CO_2 or metal ions.[11−13] For these applications of CA, enzyme-handling methods that enhance recovery and maintain catalytic activity for CO_2 conversion or even increase biosensor sensitivity are desirable to reduce the overall cost of production and to maximally harness the catalytic power of the enzyme.[14−16]

One of the ways to achieve the aforementioned goal is to immobilize CA in an oriented manner with a high density on a nanoscale support.[17] Proteins can serve as self-assembling scaffolds for the energetically favorable bottom-up fabrication of well-ordered nanomaterials with genetically encodable functionalities.[18] In particular, viral particles are naturally designed nanoscaffolds with coat protein (CP) building blocks that are capable of programmed self-assembly.[19] The oriented attachment of enzymes to virus-based particles or virus-like particles (VLPs; nanostructures that resemble the structures of viruses but lack viral genomes) has been an attractive method for the development of enzyme nanocarriers with precise positional control.[20−23]

Many plant viruses are filamentous. Filamentous structures with a high aspect ratio offer a large surface area for enzyme immobilization and provide sufficient particle size along the one-dimensional structure.[24] Most plant viruses are made up of a single type of CP,[25] enabling facile engineering of the scaffolds. Although enzymes have been successfully immobilized on plant viral scaffolds *via* bioconjugation or chemical coupling, these methods require multiple steps for conjugation and excess amounts of enzymes and toxic reagents, typically resulting in low conjugation efficiencies.[26−28] Alternatively, conjugation of enzymes by genetic fusion provides a more facile and cost-effective method for the display of enzymes on viral scaffolds, enabling one-pot production and coupling of both enzymes and scaffold proteins.[29,30] The production and assembly of plant viral CPs genetically fused with *Candida antarctica* lipase B into virus-based filamentous catalytic particles have been shown in plants.[29] However, the production of these particles requires a long time for both plant cultivation and systemic infection, and the limited host ranges of plant viruses may significantly hamper the efficient

Received: June 17, 2020
Revised: August 4, 2020
Published: August 11, 2020

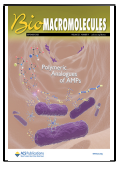

https://dx.doi.org/10.1021/acs.biomac.0c00925
Biomacromolecules 2020, 21, 3847−3856

design and production of industrially relevant catalytic nanoparticles.[31−33] Although *Escherichia coli* may be utilized as a universal bacterial host for the rapid and large-scale production of VLPs in place of the plant system,[19,34] to date, no one has reported the one-step *in vitro* assembly of catalytic VLPs using an enzyme-fused filamentous plant viral CP produced in *E. coli*.

In this study, the CA enzyme from the marine bacterium *Hydrogenovibrio marinus* (*hm*CA) was genetically fused to the CP (CP_{PVY}) of potato virus Y (PVY) to construct *in vitro* self-assembled catalytic nanofilaments for CO_2 capture with immobilized enzyme at a high density in a spatially oriented and ordered fashion along the surface of VLPs (Figure 1).

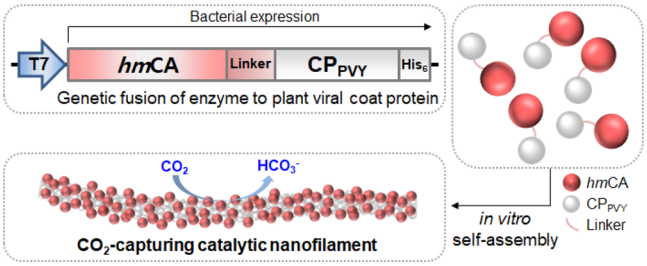

Figure 1. Schematic illustration of the production of enzyme-fused plant viral CP by bacteria and the *in vitro* assembly into catalytically active nanofilaments. *hm*CA, carbonic anhydrase from *H. marinus*; CP_{PVY}, CP of potato virus Y.

Because of the high activity and stability as well as the remarkable solubility and expression level in *E. coli*, *hm*CA has been considered an attractive enzyme for bioinspired CO_2 capture.[35−37] PVY is a flexuous filamentous plant virus belonging to the genus Potyvirus, whose near-atomic structure has been recently determined.[38] We show that CP_{PVY} with the newly identified region for internal translation initiation, combined with the designed strategies for successful assembly and stability improvement, can be used as a compelling scaffold for the engineering and *in vitro* construction of VLP-based biocatalysts.

MATERIALS AND METHODS

***E. coli* Strains and General Culture Conditions.** The strains, plasmids, and oligonucleotide primers used in this study are listed in Table S1 (Supporting Information). *E. coli* TOP10 (Thermo Fisher Scientific, USA) was used for all DNA experiments, and recombinant protein expression was performed in *E. coli* BL21(DE3) (Novagen, USA). Luria-Bertani (LB) medium supplemented with appropriate antibiotics (50 μg/mL ampicillin or 10 μg/mL streptomycin) was used for *E. coli* culture at 37 °C with shaking at 220 rpm in an incubator (Jeiotech, Korea).

Plasmid Construction. The CP_{PVY} gene (GenBank accession number: ADH52720) was codon optimized for *E. coli*, chemically synthesized (Genscript, USA), and subcloned into pET-22b (+) (Novagen, USA) using *Nde*I and *Xho*I restriction sites, resulting in pET-CP. Other plasmids containing fusion genes were constructed based on overlap polymerase chain reaction (PCR). The *hm*CA gene and CP_{PVY} gene were amplified using the template plasmids pPelB-ss::hmCA and pET-CP, respectively, and the used primers are listed in Table S1. The amplified DNA fragments were purified and mixed, and the mixture was subsequently used as a template for overlapping PCR to construct the fusion gene. The PCR product was ligated into the pGEM-T Easy vector (Promega, USA) and directly sequenced prior to subcloning into pET-22b(+) using *Nde*I and *Xho*I restriction sites. For periplasmic expression, the whole fusion gene was PCR-amplified from pET-CA-CP and cloned into pET-22b(+) using *Nco*I and *Xho*I restriction sites, resulting in pPelB-ss::CA-CP or pPelB-ss::Strep-CA-CP with N-terminal SP_{PelB}. For the construction of mutants, one-step PCR-based mutagenesis was performed using pPelB-ss::CA-CP as the template plasmid.[39] The mutations were confirmed by direct sequencing. All recombinant genes had a His_6-tag at the C terminus.

Expression and Purification of Engineered Viral CP. Recombinant *E. coli* BL21(DE3) strains transformed with the constructed plasmids were incubated in LB media supplemented with 50 μg/mL ampicillin at 37 °C in a shaking incubator. The expression of recombinant protein was induced at 0.6−0.8 OD_{600} by adding 0.1 mM isopropyl-β-D-thiogalactopyranoside (Duchefa Biochemie, Netherlands). The cells were further cultivated at 25 °C for 12 h, centrifuged at 4 °C and 4000*g* for 10 min, and resuspended in 50 mM sodium phosphate buffer supplemented with 300 mM NaCl and 10 mM imidazole (pH 8.0). Cell lysates were prepared by disrupting the cell suspensions with an ultrasonic dismembrator (Sonics and Materials, USA) for 20 min at 20% amplitude on ice water. For fractionation, the lysates were centrifuged at 4 °C and 10,000*g* for 10 min; the supernatant was designated the soluble fraction (S) while the pellet was designated the insoluble fraction (IS). The soluble fraction was mixed with Ni^{2+}-nitrilotriacetic acid agarose beads (Qiagen, USA), and the recombinant protein was purified according to manufacturer's instructions. For self-assembly, the purified protein was thoroughly dialyzed against 20 mM sodium phosphate buffer (pH 7.0) supplemented with 500 mM NaCl using a Spectra/POR dialysis membrane with a 6−8 kDa molecular weight cutoff (Spectrum Labs, USA) at 4 °C for 12 h. For tandem affinity purification using Strep-tag, the dialyzed sample was mixed with Strep-Tactin Superflow (Qiagen), and the recombinant protein was purified according to manufacturer's instructions.

Protein Gel Electrophoretic Analysis. Sample proteins were separated by sodium dodecyl sulfate−polyacrylamide gel electrophoresis (SDS-PAGE). The proteins on the gel were visualized by staining with 0.1% Coomassie Brilliant Blue R-250 (Bio-Rad, USA) in 10% acetic acid, 50% methanol, and 40% H_2O, followed by destaining with 10% acetic acid, 50% methanol, and 40% H_2O.

Protein Quantification. The purified protein sample was denatured by mixing with 8 M guanidine hydrochloride GuHCl/20 mM sodium phosphate buffer (pH 7.5) in a 1:3 volume ratio, and the absorbance of the denatured protein was measured at 280 nm in a quartz crystal cuvette. The protein molar concentration of the purified sample was determined using the measured absorbance and the calculated extinction coefficient at 280 nm by ProtParam (http://web.expasy.org/protparam/; 42,985 M^{-1} cm^{-1} for free *hm*CA, 74,260 M^{-1} cm^{-1} for *hm*CA-CP_{PVY} fusion proteins).[40] For the comparison of enzymatic activity, the enzyme concentrations of SP_{PelB}-*hm*CA-CP_{PVY} and SP_{PelB}-*hm*CA-CP^{*}_{PVY}DE were calculated based on the molar concentration of SP_{PelB}-*hm*CA-CP^{*}_{PVY} by the densitometric analysis of the band intensities on the protein gel performed using ImageJ.[41]

Transmission Electron Microscopy. Protein samples were placed on a carbon-coated copper grid and stained with 2% uranyl acetate solution. After drying for 1 h in a vacuum oven, transmission electron microscopy (TEM) was performed using FEI Tecnai T12 operating at 120 kV (FEI Company, USA).

Stability Test. One of two protein sample aliquots was incubated for 7 days at 37 °C in a water bath, and the other sample was stored at −20 °C. Protein degradation was analyzed by SDS-PAGE.

N-Terminal Amino Acid Sequencing. N-terminal amino acid sequencing was performed according to Edman degradation. The purified protein was run on SDS-PAGE gel, and the gel was blotted onto a polyvinylidene difluoride membrane (Millipore, USA); the membrane was stained with Coomassie Brilliant Blue R-250. After thorough washing, the band of interest was removed and subjected to Edman degradation using a Procise 492 sequencer (Applied Biosystems, USA).

***In Silico* Calculation.** Translation initiation rates were predicted by the RBS calculator and UTR Designer.[42,43] Protein disorder propensity was predicted by IUPred2A.[44]

https://dx.doi.org/10.1021/acs.biomac.0c00925
Biomacromolecules 2020, 21, 3847−3856

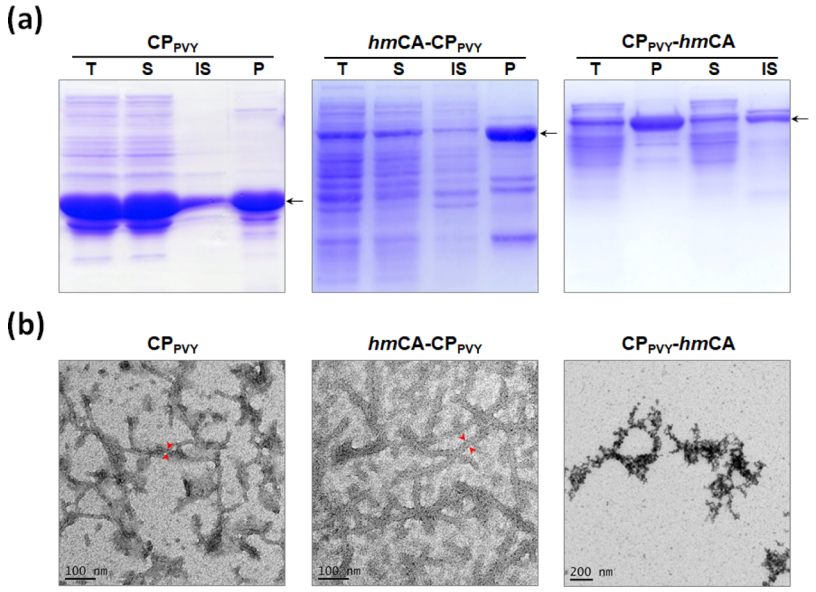

Figure 2. Effect of the fusion position of *hm*CA to CP_{PVY} on the assembly of VLPs. (a) Expression and purification of recombinant proteins. The arrow indicates the band position of each recombinant protein. Lanes: T, total cell lysate; S, soluble fraction; IS, insoluble fraction; and P, purified protein. (b) Electron micrographs of VLP formation. Red arrowheads indicate the outer edges of a VLP. The fusion proteins contain the flexible $(GGGGS)_2$ linker at the fusion junction.

Enzyme Activity Assay. CA activity was measured by CO_2 hydration assay as previously described.[36] The sample (10 μL) was mixed with 20 mM Tris buffer (pH 8.3; 600 μL) supplemented with 100 μM phenol red (Sigma-Aldrich) in a disposable cuvette. Ice-cold CO_2-saturated deionized water (400 μL) was added and rapidly mixed by thorough pipetting. The reaction was performed at 4 °C inside the spectrometer, and the time-course color change was monitored at 570 nm. The noncatalyzed reaction was also measured by adding the same amount of blank buffer instead of enzyme buffer. The time (t) required for the absorbance to decrease from 1.2 (corresponding to pH 7.5) to 0.18 (pH 6.5) was determined. The Wilbur-Anderson activity (U) is calculated by eq 1, where t_0 is the time for the noncatalyzed reaction.[36,45]

$$U = \frac{t_0 - t}{t \times 5} \tag{1}$$

Filter Trap Assay. Protein samples were filtered using a 0.2 μm cellulose acetate syringe filter (GVS Life Sciences, USA). Bovine CA (bCA) (Sigma-Aldrich) was used as a control protein. Protein concentrations or enzyme activities before (c_i) and after filtration (c_f) were measured using the Bradford reagent (Bio-Rad) or the CO_2 hydration assay, respectively. The filtered protein content (%) is calculated by eq 2.

$$\text{Filtered content (\%)} = \left(\frac{c_i - c_f}{c_i}\right) \times 100 \tag{2}$$

RESULTS AND DISCUSSION

Positional Effect of *hm*CA Fused to CP_{PVY} on the VLP Assembly. Two fusion proteins in which *hm*CA was genetically attached to either the N terminus (*hm*CA-CP_{PVY}) or C terminus (CP_{PVY}-*hm*CA) of CP_{PVY} *via* the flexible $(GGGGS)_2$ linker were constructed along with bare CP_{PVY} to investigate the positional effect of the fused enzyme on VLP assembly. The 31.1 kDa bare CP_{PVY} and 65.2 kDa *hm*CA-fused proteins were highly expressed in *E. coli* and one-step purified *via* the C-terminal hexahistidine (His_6)-tag using affinity chromatography (Figure 2a). CP_{PVY} or *hm*CA-CP_{PVY} was assembled into flexuous filamentous VLPs, while CP_{PVY}-*hm*CA only showed irregular aggregation of protein particles (Figure 2b). It has been recently revealed that the C-terminal region of CP_{PVY} is facing and completely buried in the interior of the filament while the N-terminal region of CP_{PVY} is surface exposed.[38] The bulky *hm*CA protein fused to the C terminus of each copy of CP_{PVY} would not be accommodated in the lumen of VLPs, thus preventing CP_{PVY}-*hm*CA from forming normal filamentous structures. Indeed, it has been shown that the VLP assembly can be hampered by the addition of a short linker sequence (19 amino acids) to the C terminus of CP_{PVY}.[46] Therefore, it can be concluded that VLPs can be assembled only with the N-terminal fusion of the enzyme to CP_{PVY}.

Unlike the authentic PVY particle with a length of ~730 nm,[47] the VLPs from both CP_{PVY} and *hm*CA-CP_{PVY} were heterogeneous in length as shown by TEM (Figure 2b) and dynamic light scattering analyses (Figure S1, Supporting Information), which coincides with previous observations.[38,46] The diameter of VLPs from *hm*CA-CP_{PVY} was up to 21 nm, which is much thicker than that (12 nm) of bare CP_{PVY} (Figure 2b). This result indicates that the bulky enzyme was successfully displayed on the surface of the VLPs. The VLPs from *hm*CA-CP_{PVY} were heterogeneous in diameter within a single particle, which appeared to be the result of hybrid assembly from the mixture of full length and truncated forms of *hm*CA-CP_{PVY} (see below). It is worth noting that the displayed size of *hm*CA (~34 kDa) was even larger than the size of CP_{PVY} (~31 kDa), and it is one of the largest reported proteins genetically fused to plant viral CPs.[20]

Impact of Linker Flexibility on the VLP Assembly. To assess the impact of the flexibility of the linker that connects *hm*CA to CP_{PVY} on the VLP assembly, we tested a rigid linker with a sequence of $A(EAAAK)_2A$ in addition to the previously tested flexible linker $(GGGGS)_2$.[48] A fusion protein with *hm*CA directly linked to the N terminus of CP_{PVY} without a linker was also constructed. The fusion proteins were successfully expressed and purified as soluble forms (Figure 3a). The assembly of filamentous VLPs was severely impaired

https://dx.doi.org/10.1021/acs.biomac.0c00925
Biomacromolecules 2020, 21, 3847−3856

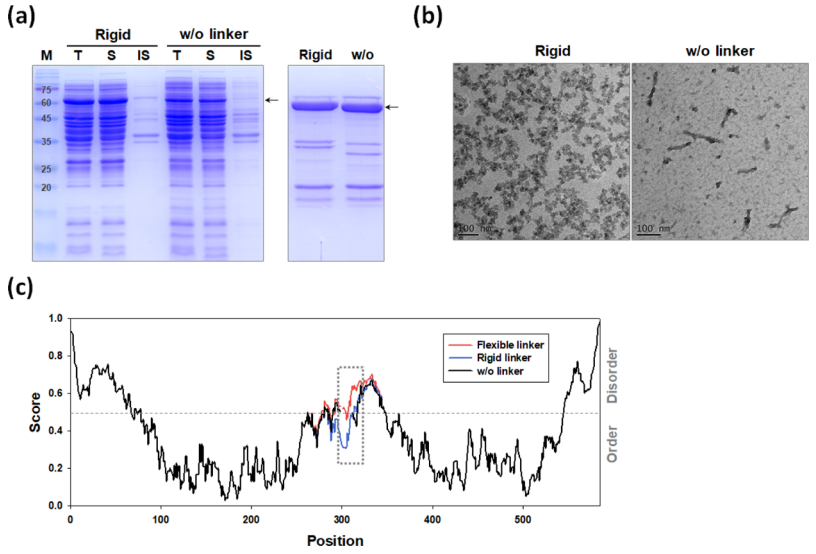

Figure 3. Effect of linker flexibility of *hm*CA-CP$_{PVY}$ on the assembly of VLPs. (a) (Left) Expression and (Right) purification of *hm*CA-CP$_{PVY}$ with the rigid linker A(EAAAK)$_2$A or without a linker. The arrow indicates the band position of the recombinant fusion protein. Lanes: *M*, molecular mass marker (kDa); T, total cell lysate; S, soluble fraction; and IS, insoluble fraction. (b) Electron micrographs of VLP formation. (c) Protein disorder propensity predicted by IUPred2A. The fusion junction is highlighted in a gray dotted box. The position numbering follows the numbering system of *hm*CA-CP$_{PVY}$ with the rigid linker that has more residues than the other two fusion proteins do. The graph for *hm*CA-CP$_{PVY}$ with a flexible linker or without a linker is broken with a gap after the end of the *hm*CA sequence and is shifted toward the right to align the remaining C-terminal regions and facilitate the comparisons.

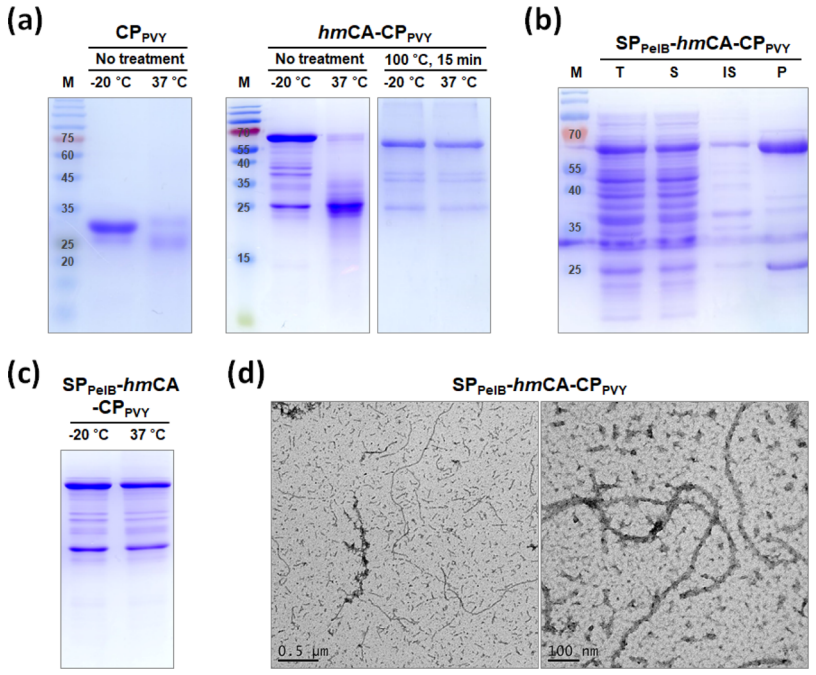

Figure 4. Improved stability of *hm*CA-CP$_{PVY}$ against degradation by periplasmic translocation. (a) Proteolytic degradation of purified protein analyzed by SDS-PAGE. Samples were incubated (or stored) at the indicated temperature for 7 days. (b) Expression and purification of SP$_{PelB}$-*hm*CA-CP$_{PVY}$. Lanes: *M*, molecular mass marker (kDa); T, total cell lysate; S, soluble fraction; IS, insoluble fraction; and P, purified protein. (c) Stability of SP$_{PelB}$-*hm*CA-CP$_{PVY}$ against degradation. (d) Electron micrographs of SP$_{PelB}$-*hm*CA-CP$_{PVY}$ VLPs.

by the use of the rigid linker as opposed to the case of the flexible linker, resulting in round-shaped particles with a diameter of 15−18 nm that further aggregated into clumps (Figure 3b). Interestingly, the fusion protein without a linker was also capable of VLP formation, although most of the assembled particles were rodlike with shorter lengths. The local flexibility near the fusion junction of the fusion protein with the rigid linker was predicted to be significantly reduced compared to that of the fusion protein without a linker while the introduction of the flexible linker increased the local flexibility (Figure 3c). Thus, increasing flexibility near the fusion junction seems to be critical for the successful construction of enzyme-displaying nanofilaments using CP$_{PVY}$.

Improved Stability of VLPs by Periplasmic Translocation of *hm*CA-CP$_{PVY}$. After incubating the purified *hm*CA-CP$_{PVY}$ at 37 °C for a long time (7 days), unexpected

https://dx.doi.org/10.1021/acs.biomac.0c00925
Biomacromolecules 2020, 21, 3847−3856

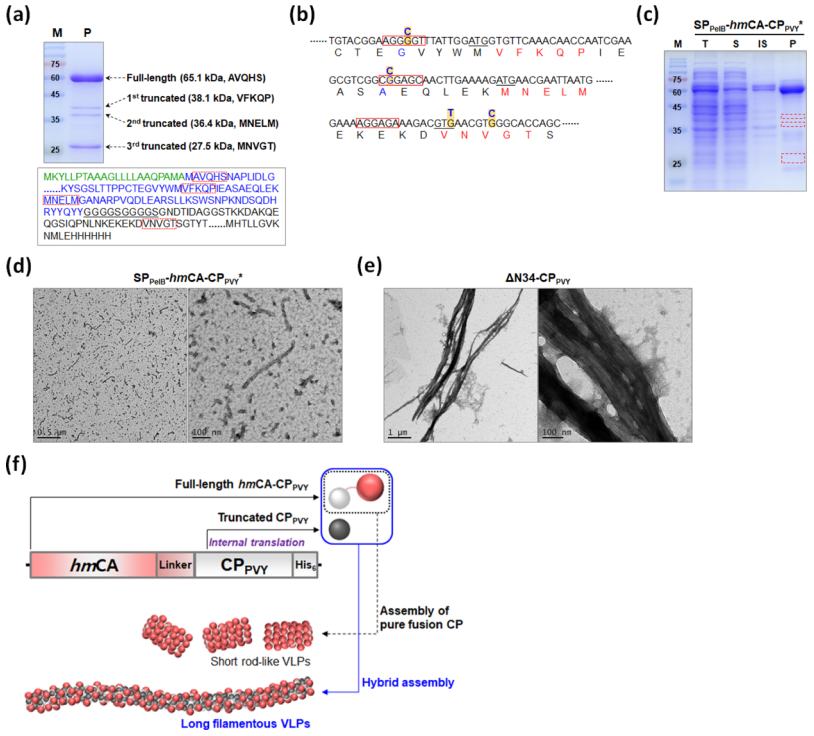

Figure 5. Involvement of truncated forms in filamentous VLP formation revealed by the introduction of silent mutations. (a) (Upper) N-terminal sequence analysis of truncated proteins and (Lower) the corresponding regions (boxed in red dotted lines) in the SP_{PelB}-*hm*CA-CP_{PVY} sequence. The SP_{PelB}, *hm*CA, and CP_{PVY} sequences are indicated in green, blue, and black, respectively. The linker sequence is underlined. (b) Nucleotide positions for silent mutations. The N-terminal sequences of truncated proteins are in red. Each start codon for internal translation initiation is underlined. Putative Shine−Dalgarno sequences are boxed in red. The positions of silent mutations are boxed in yellow. The introduced sequences are in blue. (c) Expression and purification of the mutant (*) of SP_{PelB}-*hm*CA-CP_{PVY}. The disappeared band positions in SDS-PAGE are boxed in red dotted lines. Lanes: *M*, molecular mass marker (kDa); T, total cell lysate; S, soluble fraction; IS, insoluble fraction; and P, purified protein. Electron micrographs of (d) SP_{PelB}-*hm*CA-CP^{*}_{PVY} VLPs and (e) ΔN34-CP_{PVY} VLPs. (f) Schematic diagram of filamentous VLP formation assisted by the hybrid assembly of truncated CP_{PVY} with *hm*CA-CP_{PVY}, leading to the partial decoration of VLPs with the enzyme.

degradation of the fusion protein was observed (Figure 4a). A similar degradation was also observed for bare CP_{PVY} (Figure 4a). When the *hm*CA-CP_{PVY} sample was incubated under the same conditions after brief boiling at 100 °C, the protein remained intact without degradation, suggesting the involvement of biological protease(s) in degradation (Figure 4a). Although this type of instability of recombinant VLPs has rarely been investigated,[32] improvement of the stability against proteolytic degradation would be an important prerequisite for future applications of enzyme-tethered nanofilaments.

The column was thoroughly washed during the His_6-tag affinity purification of protein to remove nonspecifically bound proteins but this was not effective in reducing the degradation (data not shown); we suspected that the contaminating proteases, originating from *E. coli* cytoplasm, were encapsulated within the lumen of some VLPs formed inside the cell and copurified along with the recombinant fusion protein. In contrast to the interior of authentic PVY filaments filled with a compact cone-shaped structure composed of the C-terminal region of CP_{PVY} along with viral RNA, the interior of CP_{PVY} VLPs seems to be rather hollow with a flexible C-terminal region without any defined structure.[38] This feature could occasionally allow some guest molecules (proteases) to be contained in the 4.5 nm-wide lumen of VLPs. The use of protease inhibitors might be effective in reducing the degradation; however, it cannot be a fundamental solution. To tackle the degradation problem, the fusion protein was secreted into the periplasm of *E. coli* because the periplasmic space contains fewer amounts and types of proteases compared to the cytoplasm.[49] We exploited the widely used signal peptide of PelB (SP_{PelB}) that directs protein secretion *via* the Sec pathway. Unlike the Tat pathway, in the Sec pathway, protein folding occurs only after the protein is exported to the periplasm,[49] which avoids the cytoplasmic assembly of VLPs and concomitant encapsulation of undesirable proteases. The periplasmic expression and purification of *hm*CA-CP_{PVY} were successful (Figure 4b), and signal cleavage was confirmed by N-terminal sequencing (Figure 5a). Remarkably, the purified protein remained stable without a sign of degradation even after 7 days of incubation at 37 °C (Figure 4c). The formation of nanofilaments was also observed using periplasmic *hm*CA-CP_{PVY} (Figure 4d). Although the expression level of periplasmic *hm*CA-CP_{PVY} was lower compared to that of cytoplasmic *hm*CA-CP_{PVY}, the specific activity of the purified VLPs was 2.6-fold higher (Figure S2, Supporting Information), presumably because of the correct folding of disulfide-bonded *hm*CA promoted in the periplasm.[36] In addition, the amount of long filamentous VLPs from periplasmic *hm*CA-CP_{PVY}, which was roughly assessed by filter trap assay (see below), was similar to that from the cytoplasmic counterpart (Figure S2). Thus, the periplasmic expression of enzyme-fused CP_{PVY} can be a powerful strategy and might be applied to other viral CPs to improve the stability of VLPs against endogenous proteolytic degradation.

Hybrid Assembly of Full Length and Truncated Forms of *hm*CA-CP_{PVY}. In addition to the major band

https://dx.doi.org/10.1021/acs.biomac.0c00925
Biomacromolecules 2020, 21, 3847−3856

corresponding to *hm*CA-CP$_{PVY}$, three minor yet clear bands with smaller sizes compared to *hm*CA-CP$_{PVY}$ were consistently observed in the protein gel analysis of the purified protein (Figure 5a). Because these proteins were copurified along with full-length *hm*CA-CP$_{PVY}$, they were initially assumed to be His$_6$-tag-harboring C-terminal fragments of *hm*CA-CP$_{PVY}$ resulting from proteolytic cleavage occurring before purification. These bands did not disappear even after the purified sample was dialyzed using a 1000 kDa cutoff membrane (data not shown), implying the complexation of the truncated proteins with VLPs. When the five N-terminal amino acids of each truncated protein were sequenced by Edman degradation, it was clearly revealed that the third truncated form with the N-terminal sequence of MNVGT was not the product of proteolytic cleavage because the first amino acid methionine (Met) did not correspond to the first GTG codon for valine (Figure 5a,b). The N-terminal sequence of the other two (the first and second) truncated forms also started with or immediately after Met (Figure 5b). Because the GTG codon can be used as an alternative start codon encoding formylmethionine (fMet) and a cellular enzyme can remove fMet posttranslationally,[50,51] the three truncated forms were supposed to be generated by internal translation initiation, not by proteolytic cleavage. *In silico* predictions of the translation initiation rate show that the three minor proteins can be expressed at relatively high levels (Table 1).

Table 1. Changes in Expression Levels of Truncated Forms after Introduction of Silent Mutations

	predicted translation initiation rate or expression level[a]			
	RBS calculator		UTR designer	
	before	after	before	after
full-length	33,497	33,497	570,446	570,446
1st truncated	72	23	57,587	3716
2nd truncated	1098	94	20,902	1835
3rd truncated	2616	ND	47,712	ND

[a]The values are presented in an arbitrary unit for each prediction method. ND = not detected.

To improve the sample purity by eliminating or reducing the undesirable expression of the truncated forms of *hm*CA-CP$_{PVY}$, silent mutations were designed and introduced into the putative Shine−Dalgarno sequences (for the first and second truncated forms) and the Val codons (for the third truncated form) without altering the protein sequence of *hm*CA-CP$_{PVY}$ (Figure 5b, Table 1). No apparent bands corresponding to the three truncated forms were observed based on the gel analysis of the *hm*CA-CP$^{*}_{PVY}$ mutant expressed in the periplasm (Figure 5c), indicating that the minor proteins were actually synthesized because of internal translation initiation, as expected. However, long filamentous VLPs were not observed in the electron microscopic analysis, and only short rod-shaped fragments were predominant (Figure 5d). This result indicates that the removed minor protein(s) were essentially required for the successful formation of filamentous VLPs. Among the truncated forms, the third is a truncated CP$_{PVY}$ with 34 amino acids deleted from the N terminus (Figure 5a), which has been previously misidentified as a cleavage product.[46] When this third truncated protein (ΔN34-CP$_{PVY}$) was separately expressed, it could form long filamentous VLPs that further assembled into thick nanofibrils by side-by-side aligned stacking (Figure 5e). This result implies that the third truncated protein could coassemble with the full length and truncated forms of *hm*CA-CP$_{PVY}$ into long filaments in a hybrid manner, relieving steric hindrance (Figure 5f). In contrast, it seemed that the assembly of the pure *hm*CA-CP$^{*}_{PVY}$ mutant was severely hampered because of cumulative steric hindrance by the bulky *hm*CA moiety, resulting in the formation of only short VLPs.

To demonstrate the coassembly, a dual-tagging system was constructed by adding Strep-tag to the N terminus of *hm*CA-CP$_{PVY}$. The assembled proteins purified using His$_6$-tag were used for the second purification using Strep-tag. The final purified sample still showed the same band pattern of the truncated proteins in SDS-PAGE analysis (Figure 6a). Because only the full-length *hm*CA-CP$_{PVY}$ possesses the N-terminal Strep-tag, the result indicates that the truncated proteins were coassembled along with the full-length *hm*CA-CP$_{PVY}$. Next, we further tested the hybrid assembly by mixing the cell lysates of SP$_{PelB}$-*hm*CA-CP$^{*}_{PVY}$ and ΔN34-CP$_{PVY}$ with different volume mixing ratios. After purification of the recombinant proteins from the mixed cell lysate (Figure 6b), the amount of long filamentous VLP formation was estimated by the filter trap assay, where the filtered content of proteins after filtration using a 0.2 μm syringe filter was measured by Bradford assay

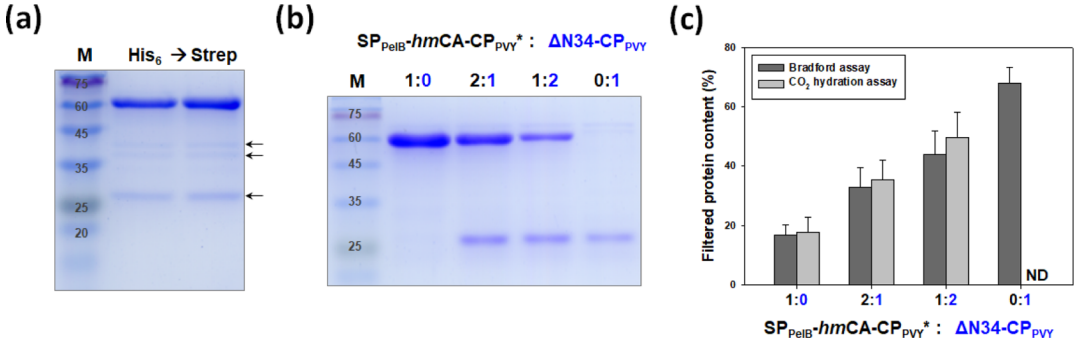

Figure 6. Probing the *in vitro* hybrid assembly. (a) Tandem affinity purification of SP$_{PelB}$-Strep-*hm*CA-CP$_{PVY}$ using the C-terminal His$_6$-tag and the N-terminal Strep-tag analyzed by SDS-PAGE. The arrows indicate the band positions of the three truncated forms. (b) Purified proteins from the mixture of SP$_{PelB}$-*hm*CA-CP$^{*}_{PVY}$ and ΔN34-CP$_{PVY}$ cell lysates analyzed by SDS-PAGE. The mixing ratio of the lysates is indicated on each lane. *M*, molecular mass marker (kDa). (c) Protein contents of the purified proteins after passing through a 0.2 μm filter, analyzed by protein quantification (Bradford assay) and enzymatic activity (CO_2 hydration assay). Error bars represent standard deviations from three independent experiments. ND = not detected.

https://dx.doi.org/10.1021/acs.biomac.0c00925
Biomacromolecules 2020, 21, 3847−3856

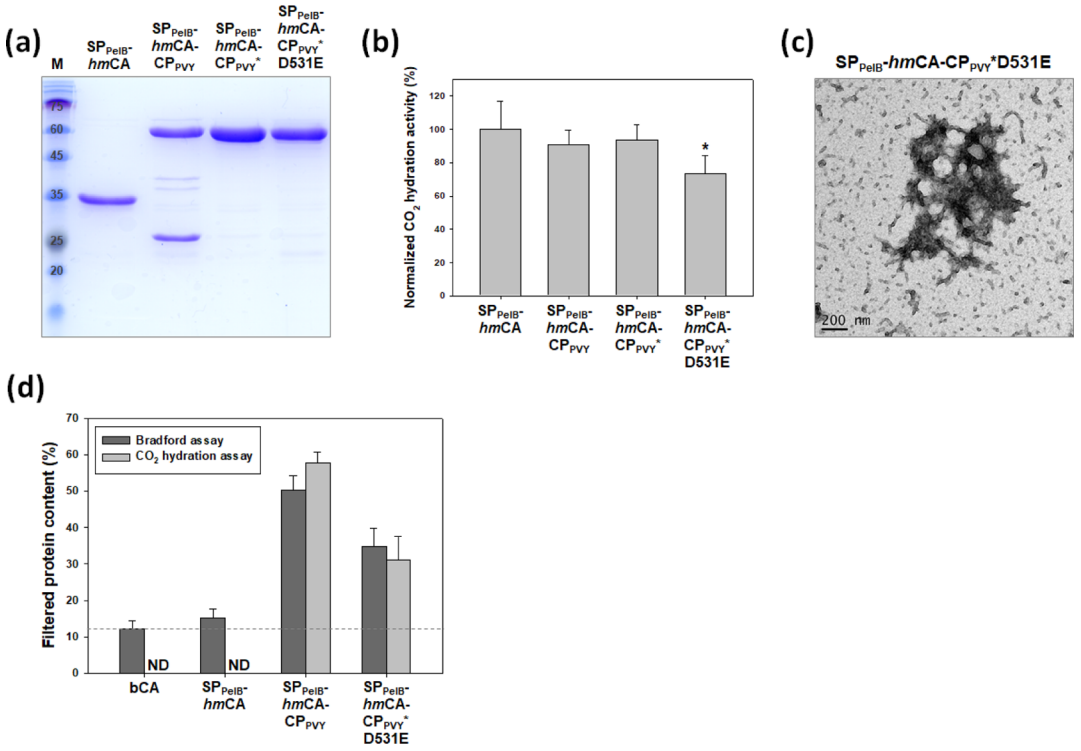

Figure 7. Effect of the ordered assembly on catalytic activity and protein recovery. (a) Coomassie blue-stained SDS-PAGE gel for densitometric quantification of purified proteins. *M*, molecular mass marker (kDa). (b) CO_2 hydration activities of purified enzymes normalized to the activity of free *hm*CA (SP_{PelB}-*hm*CA). The activities were represented based on the same molar amount of enzymes. Error bars represent standard deviations from three independent experiments. Asterisks indicate statistical significance of the D531E mutant compared with the other samples determined by *t*-test (*$p < 0.05$). (c) Electron micrograph of SP_{PelB}-*hm*CA-CP^{*}_{PVY}D531E aggregates. (d) Protein contents of purified enzymes after passing through a 0.2 μm filter analyzed by protein quantification (Bradford assay) and enzymatic activity (CO_2 hydration assay). ND = not determined. bCA, a monomeric protein, was used as a control. Error bars represent standard deviations from three independent experiments.

and CO_2 hydration assay (Figure 6c). As expected, the filtered content of proteins was higher when the ratio of ΔN34-CP_{PVY} to SP_{PelB}-*hm*CA-CP^{*}_{PVY} was higher, implying that ΔN34-CP_{PVY} was the component responsible for the formation of larger VLPs. More importantly, the enzymatic CO_2 hydration activities of filtered protein contents were linearly proportional to the relative amounts of filtered proteins (Figure 6c). Because ΔN34-CP_{PVY} showed no enzymatic activity, and the filtered content of the pure SP_{PelB}-*hm*CA-CP^{*}_{PVY} (16.9%) was relatively low (Figure 6c), it can be concluded that the catalytic sites of SP_{PelB}-*hm*CA-CP^{*}_{PVY} proteins were evenly distributed into the various sizes of VLPs along with ΔN34-CP_{PVY} *via* the hybrid assembly. The result also demonstrates that the hybrid assembly could occur *in vitro* after the cell lysis.

The 2A sequence originating from the foot-and-mouth disease virus has been effectively exploited in plants to produce a mixture of bare CP and fused CP from a single gene construct, reducing steric hindrance and thus facilitating the self-assembly of target protein-displaying VLPs.[19,29,31,52] Similarly, the third site for internal translation initiation identified in our study is valuable for the successful *in vitro* hybrid assembly of enzyme-tethered CP_{PVY} VLPs. In addition, the translation initiation rate for the third region can be easily fine-tuned by synthetic biology approaches,[42,43,53] which may allow the VLP surface to be decorated with a controllable density of enzymes or much larger proteins to be displayed. Therefore, the internal translation region can be considered a naturally occurring, bacterial alternative version of the 2A sequence that can be further engineered for future applications.

Catalytic Activity for CO_2 Hydration and Recovery Potential of *hm*CA-CP_{PVY} VLPs. The catalytic activities of the constructed nanoparticles were measured by CO_2 hydration assay. Free *hm*CA (SP_{PelB}-*hm*CA) was also tested as a positive control. Because the purified fusion proteins actually had different degrees of purity (Figure 7a), the measured enzymatic activities of the samples were corrected according to the enzyme concentrations that were calculated by the densitometric analysis of the intensities of the major fusion protein bands on the gel, based on the assumption that SP_{PelB}-*hm*CA and SP_{PelB}-*hm*CA-CP^{*}_{PVY} samples are pure. The specific activity of free *hm*CA was determined to be 2,970 U/mg, which coincides with a previous report.[36] The relative specific activities of SP_{PelB}-*hm*CA-CP_{PVY} (90.6%) and SP_{PelB}-*hm*CA-CP^{*}_{PVY} (93.3%) were comparable to that of free *hm*CA (Figure 7b). The high retention of activity of the fusion proteins implies that neither the conjugation to CP_{PVY} by genetic fusion nor the assembly of enzymes itself affected the enzymatic performance of *hm*CA. Compared to the dispersed free-enzyme system, the assembled enzymes that highly condensed in a localized space might experience a relative reduction in the rate of substrate diffusion, leading to slightly lower activity in the diffusion-controlled, CA-catalyzed CO_2 hydration reaction.

To assess the effect of the ordered assembly on catalytic activity, we created an assembly-deficient mutant by the introduction of an additional mutation, D531E, on SP_{PelB}-*hm*CA-CP^{*}_{PVY}. The Asp^{531} residue (Asp^{201} in the wild-type PVY) corresponds to the Asp^{238} and Asp^{198} residues in

https://dx.doi.org/10.1021/acs.biomac.0c00925
Biomacromolecules 2020, 21, 3847−3856

Johnsongrass mosaic virus CP and tobacco etch virus CP, respectively. When this conserved residue was mutated to Glu, the potyviral CPs lost the capability of ordered self-assembly without compromising the overall protein structural integrity.[54,55] Similarly, the purified D531E mutant showed irregular protein aggregates and did not form filamentous structures (Figure 7a,c). Notably, the mutant D531E exhibited only 73.1% of the free-enzyme activity (Figure 7b). In contrast to the ordered assembly of catalytic sites on the surface of VLPs, some of the active sites of the D531E mutant might be buried and shielded by neighboring subunits, resulting in reduced substrate accessibility and, in turn, lower catalytic efficiency.[56] Thus, this result demonstrates the importance of the surface-oriented and ordered assembly to ensure high activity of the catalytic nanofilaments.

Finally, the recovery potential of the nanofilaments was evaluated by the filter trap assay (Figure 7d). bCA, a well-known monomeric enzyme,[57] was used as a control. A small fraction (15.1%) of free *hm*CA was retained on the filter membrane, similar to the case of bCA (12.3%), indicating the basal level of nonspecific protein adsorption to the membrane material. In contrast, a much higher content of SP_{PelB}-*hm*CA-CP_{PVY} was retained after filtration (50.3% by Bradford assay and 57.7% by activity assay), which was also significantly higher than that of SP_{PelB}-*hm*CA-CP^{*}_{PVY} (16.9% by Bradford assay and 17.8% by activity assay) (Figure 6c). This result confirms the previous observation that the particle size of long filamentous VLPs constructed from the hybrid assembly was larger than short rodlike VLP assembled from the pure *hm*CA-CP^{*}_{PVY} mutant. The D531E mutant showed a relatively high retainment (34.8% by Bradford assay and 31.1% by activity assay), presumably because of the formation of large aggregates (Figure 7c). The particle size of the nanofilaments was greater than that of free enzyme, which can facilitate its recovery and reuse in potential biocatalytic systems, for example, in an enzyme membrane reactor where, unlike free enzyme that requires ultrafiltration or nanofiltration membranes with small pore sizes for enzyme reuse, membranes with larger pore size might be employed without enzyme loss to reduce operating cost and increase mass transfer.[58,59] Collectively, the *in vitro* assembled, enzyme-decorated nanofilament can be used as an efficient biocatalyst with high activity and recovery potential.

CONCLUSIONS

The bacterial production and *in vitro* self-assembly of engineered plant viral CP into catalytic nanofilaments were successfully demonstrated using *hm*CA fused to N terminus of CP_{PVY} *via* a flexible linker. Improved stability of VLPs against endogenous proteolytic degradation was attained by periplasmic secretion of the fusion protein. The importance of coexpressed truncated forms was revealed by the introduction of silent mutations, demonstrating that the hybrid assembly was essential for the successful formation of filamentous VLPs by alleviating steric hindrance. The VLPs showed CO_2 hydration activity comparable to that of free enzyme owing to the oriented and ordered immobilization of enzyme on the surface of nanofilaments. Compared to free enzymes, the nanofilaments were larger in size, allowing them to be efficiently used and recovered for potential bioconversion processes. Further engineering of CP_{PVY}, especially the region for internal translation initiation, would enable the conjugation of enzymes with various sizes with a controllable density.

ASSOCIATED CONTENT

Supporting Information

The Supporting Information is available free of charge at https://pubs.acs.org/doi/10.1021/acs.biomac.0c00925.

Size distributions of VLPs measured by DLS; comparison of cytoplasmic *hm*CA-CP_{PVY} with the periplasmic counterpart in terms of expression level, activity, and VLP assembly; and *E. coli* strains, plasmids, and oligonucleotide primers used in this study (PDF)

AUTHOR INFORMATION

Corresponding Author

Byung Hoon Jo − *Division of Life Science and Research Institute of Life Science, Gyeongsang National University, Jinju 52828, Korea;* orcid.org/0000-0002-6408-4317; Email: jobh@gnu.ac.kr

Authors

Suhan Wi − *Division of Applied Life Science (BK21 Plus), Gyeongsang National University, Jinju 52828, Korea*

In Seong Hwang − *Division of Applied Life Science (BK21 Plus), Gyeongsang National University, Jinju 52828, Korea*

Complete contact information is available at: https://pubs.acs.org/10.1021/acs.biomac.0c00925

Notes

The authors declare no competing financial interest.

ACKNOWLEDGMENTS

This work was supported by the Korea Institute of Energy Technology Evaluation and Planning (KETEP) grant (20182010600430) funded by the Ministry of Trade, Industry, and Energy, Korea, and by the National Research Foundation grant (NRF-2019R1F1A1063181) funded by the Ministry of Science and ICT, Korea.

REFERENCES

(1) Smith, K. S.; Ferry, J. G. Prokaryotic Carbonic Anhydrases. *FEMS Microbiol. Rev.* **2000**, *24*, 335−366.

(2) De Luca, V.; Vullo, D.; Scozzafava, A.; Carginale, V.; Rossi, M.; Supuran, C. T.; Capasso, C. An α-Carbonic Anhydrase from the Thermophilic Bacterium Sulphurihydrogenibium azorense is the Fastest Enzyme Known for the CO_2 Hydration Reaction. *Bioorg. Med. Chem.* **2013**, *21*, 1465−1469.

(3) Savile, C. K.; Lalonde, J. J. Biotechnology for the Acceleration of Carbon Dioxide Capture and Sequestration. *Curr. Opin. Biotechnol.* **2011**, *22*, 818−823.

(4) Bond, G. M.; Stringer, J.; Brandvold, D. K.; Simsek, F. A.; Medina, M.-G.; Egeland, G. Development of Integrated System for Biomimetic CO_2 Sequestration Using the Enzyme Carbonic Anhydrase. *Energy Fuels* **2001**, *15*, 309−316.

(5) Qi, G.; Liu, K.; House, A.; Salmon, S.; Ambedkar, B.; Frimpong, R. A.; Remias, J. E.; Liu, K. Laboratory to Bench-Scale Evaluation of an Integrated CO_2 Capture System Using a Thermostable Carbonic Anhydrase Promoted K_2CO_3 Solvent with Low Temperature Vacuum Stripping. *Appl. Energy* **2018**, *209*, 180−189.

(6) Power, I. M.; Harrison, A. L.; Dipple, G. M. Accelerating Mineral Carbonation Using Carbonic Anhydrase. *Environ. Sci. Technol.* **2016**, *50*, 2610−2618.

(7) Jo, B. H.; Seo, J. H.; Yang, Y. J.; Baek, K.; Choi, Y. S.; Pack, S. P.; Oh, S. H.; Cha, H. J. Bioinspired Silica Nanocomposite with Autoencapsulated Carbonic Anhydrase as a Robust Biocatalyst for CO_2 Sequestration. *ACS Catal.* **2014**, *4*, 4332−4340.

(8) Srikanth, S.; Alvarez-Gallego, Y.; Vanbroekhoven, K.; Pant, D. Enzymatic Electrosynthesis of Formic Acid through Carbon Dioxide Reduction in a Bioelectrochemical System: Effect of Immobilization and Carbonic Anhydrase Addition. *ChemPhysChem* **2017**, *18*, 3174−3181.
(9) Hong, S.-G.; Jeon, H.; Kim, H. S.; Jun, S.-H.; Jin, E.; Kim, J. One-Pot Enzymatic Conversion of Carbon Dioxide and Utilization for Improved Microbial Growth. *Environ. Sci. Technol.* **2015**, *49*, 4466−4472.
(10) Chen, P.-H.; Liu, H.-L.; Chen, Y.-J.; Cheng, Y.-H.; Lin, W.-L.; Yeh, C.-H.; Chang, C.-H. Enhancing CO_2 Bio-Mitigation by Genetic Engineering of Cyanobacteria. *Energy Environ. Sci.* **2012**, *5*, 8318−8327.
(11) Cammaroto, C.; Diliberto, L.; Ferralis, M.; Manca, R.; Sanna, A.; Giordano, M. Use of Carbonic Anhydrase in Electrochemical Biosensors for Dissolved CO_2. *Sens. Actuators, B* **1998**, *48*, 439−447.
(12) McCranor, B. J.; Szmacinski, H.; Zeng, H. H.; Stoddard, A. K.; Hurst, T.; Fierke, C. A.; Lakowicz, J. R.; Thompson, R. B. Fluorescence Lifetime Imaging of Physiological Free Cu(II) Levels in Live Cells with a Cu(II)-Selective Carbonic Anhydrase-Based Biosensor. *Metallomics* **2014**, *6*, 1034−1042.
(13) Fierke, C. A.; Thompson, R. B. Fluorescence-Based Biosensing of Zinc Using Carbonic Anhydrase. *BioMetals* **2001**, *14*, 205−222.
(14) Shanbhag, B. K.; Liu, B.; Fu, J.; Haritos, V. S.; He, L. Self-Assembled Enzyme Nanoparticles for Carbon Dioxide Capture. *Nano Lett.* **2016**, *16*, 3379−3384.
(15) Patel, A. N.; Anne, A.; Chovin, A.; Demaille, C.; Grelet, E.; Michon, T.; Taofifenua, C. Scaffolding of Enzymes on Virus Nanoarrays: Effects of Confinement and Virus Organization on Biocatalysis. *Small* **2017**, *13*, 1603163.
(16) Torbensen, K.; Patel, A. N.; Anne, A.; Chovin, A.; Demaille, C.; Bataille, L.; Michon, T.; Grelet, E. Immuno-Based Molecular Scaffolding of Glucose Dehydrogenase and Ferrocene Mediator on fd Viral Particles Yields Enhanced Bioelectrocatalysis. *ACS Catal.* **2019**, *9*, 5783−5796.
(17) Kim, J.; Grate, J. W.; Wang, P. Nanobiocatalysis and Its Potential Applications. *Trends Biotechnol.* **2008**, *26*, 639−646.
(18) Glover, D. J.; Giger, L.; Kim, S. S.; Naik, R. R.; Clark, D. S. Geometrical Assembly of Ultrastable Protein Templates for Nanomaterials. *Nat. Commun.* **2016**, *7*, 11771.
(19) Wen, A. M.; Steinmetz, N. F. Design of Virus-Based Nanomaterials for Medicine, Biotechnology, and Energy. *Chem. Soc. Rev.* **2016**, *45*, 4074−4126.
(20) Cardinale, D.; Carette, N.; Michon, T. Virus Scaffolds as Enzyme Nano-Carriers. *Trends Biotechnol.* **2012**, *30*, 369−376.
(21) Jordan, P. C.; Patterson, D. P.; Saboda, K. N.; Edwards, E. J.; Miettinen, H. M.; Basu, G.; Thielges, M. C.; Douglas, T. Self-Assembling Biomolecular Catalysts for Hydrogen Production. *Nat. Chem.* **2016**, *8*, 179−185.
(22) Patterson, D. P.; Prevelige, P. E.; Douglas, T. Nanoreactors by Programmed Enzyme Encapsulation Inside the Capsid of the Bacteriophage P22. *ACS Nano* **2012**, *6*, 5000−5009.
(23) Uchida, M.; McCoy, K.; Fukuto, M.; Yang, L.; Yoshimura, H.; Miettinen, H. M.; LaFrance, B.; Patterson, D. P.; Schwarz, B.; Karty, J. A.; Prevelige, P. E.; Lee, B.; Douglas, T. Modular Self-Assembly of Protein Cage Lattices for Multistep Catalysis. *ACS Nano* **2018**, *12*, 942−953.
(24) Röder, J.; Dickmeis, C.; Commandeur, U. Small, Smaller, Nano: New Applications for Potato Virus X in Nanotechnology. *Front. Plant Sci.* **2019**, *10*, 158.
(25) Yazdani, R.; Shams-Bakhsh, M.; Hassani-Mehraban, A.; Arab, S. S.; Thelen, N.; Thiry, M.; Crommen, J.; Fillet, M.; Jacobs, N.; Brans, A.; Servais, A.-C. Production and characterization of virus-like particles of grapevine fanleaf virus presenting L2 epitope of human papillomavirus minor capsid protein. *BMC Biotechnol.* **2019**, *19*, 81.
(26) Röder, J.; Fischer, R.; Commandeur, U. Engineering Potato Virus X Particles for a Covalent Protein Based Attachment of Enzymes. *Small* **2017**, *13*, 1702151.
(27) Koch, C.; Wabbel, K.; Eber, F. J.; Krolla-Sidenstein, P.; Azucena, C.; Gliemann, H.; Eiben, S.; Geiger, F.; Wege, C. Modified TMV Particles as Beneficial Scaffolds to Present Sensor Enzymes. *Front. Plant Sci.* **2015**, *6*, 1137.
(28) Cuenca, S.; Mansilla, C.; Aguado, M.; Yuste-Calvo, C.; Sanchez, F.; Sanchez-Montero, J. M.; Ponz, F. Nanonets Derived from Turnip Mosaic Virus as Scaffolds for Increased Enzymatic Activity of Immobilized Candida antarctica Lipase B. *Front. Plant Sci.* **2016**, *7*, 464.
(29) Carette, N.; Engelkamp, H.; Akpa, E.; Pierre, S. J.; Cameron, N. R.; Christianen, P. C. M.; Maan, J. C.; Thies, J. C.; Weberskirch, R.; Rowan, A. E.; Nolte, R. J. M.; Michon, T.; Van Hest, J. C. M. A Virus-Based Biocatalyst. *Nat. Nanotechnol.* **2007**, *2*, 226−229.
(30) Rao, G.; Fu, Y.; Li, N.; Yin, J.; Zhang, J.; Wang, M.; Hu, Z.; Cao, S. Controllable Assembly of Flexible Protein Nanotubes for Loading Multifunctional Modules. *ACS Appl. Mater. Interfaces* **2018**, *10*, 25135−25145.
(31) Cruz, S. S.; Chapman, S.; Roberts, A. G.; Roberts, I. M.; Prior, D. A.; Oparka, K. J. Assembly and Movement of a Plant Virus Carrying a Green Fluorescent Protein Overcoat. *Proc. Natl. Acad. Sci. U.S.A.* **1996**, *93*, 6286−6290.
(32) Werner, S.; Marillonnet, S.; Hause, G.; Klimyuk, V.; Gleba, Y. Immunoabsorbent Nanoparticles Based on a Tobamovirus Displaying Protein A. *Proc. Natl. Acad. Sci. U.S.A.* **2006**, *103*, 17678−17683.
(33) Moury, B.; Fabre, F.; Hébrard, E.; Froissart, R. Determinants of Host Species Range in Plant Viruses. *J. Gen. Virol.* **2017**, *98*, 862−873.
(34) Glasgow, J.; Tullman-Ercek, D. Production and Applications of Engineered Viral Capsids. *Appl. Microbiol. Biotechnol.* **2014**, *98*, 5847−5858.
(35) Jo, B. H.; Im, S.-K.; Cha, H. J. Halotolerant Carbonic Anhydrase with an Unusual N-Terminal Extension from a Marine Bacterium as a Novel Biocatalyst for CO Capture under High-Salt Environment. *J. CO2 Util.* **2018**, *26*, 415−424.
(36) Jo, B. H.; Moon, H.; Cha, H. J. Engineering the Genetic Components of a Whole-Cell Catalyst for Improved Enzymatic CO_2 Capture and Utilization. *Biotechnol. Bioeng.* **2020**, *117*, 39−48.
(37) Moon, H.; Kim, S.; Jo, B. H.; Cha, H. J. Immobilization of Genetically Engineered Whole-Cell Biocatalysts with Periplasmic Carbonic Anhydrase in Polyurethane Foam for Enzymatic CO_2 Capture and Utilization. *J. CO2 Util.* **2020**, *39*, 101172.
(38) Kežar, A.; Kavcic, L.; Polak, M.; Novacek, J.; Gutierrez-Aguirre, I.; Znidaric, M. T.; Coll, A.; Stare, K.; Gruden, K.; Ravnikar, M.; Pahovnik, D.; Zagar, E.; Merzel, F.; Anderluh, G.; Podobnik, M. Structural Basis for the Multitasking Nature of the Potato Virus Y Coat Protein. *Sci. Adv.* **2019**, *5*, No. eaaw3808.
(39) Urban, A.; Neukirchen, S.; Jaeger, K. E. A Rapid and Efficient Method for Site-Directed Mutagenesis Using One-Step Overlap Extension PCR. *Nucleic Acids Res.* **1997**, *25*, 2227−2228.
(40) Wilkins, M. R.; Gasteiger, E.; Bairoch, A.; Sanchez, J. C.; Williams, K. L.; Appel, R. D.; Hochstrasser, D. F. Protein Identification and Analysis Tools in the ExPASy Server. *Methods Mol. Biol.* **1999**, *112*, 531−552.
(41) Schneider, C. A.; Rasband, W. S.; Eliceiri, K. W. NIH Image to ImageJ: 25 Years of Image Analysis. *Nat. Methods* **2012**, *9*, 671−675.
(42) Salis, H. M.; Mirsky, E. A.; Voigt, C. A. Automated Design of Synthetic Ribosome Binding Sites to Control Protein Expression. *Nat. Biotechnol.* **2009**, *27*, 946−950.
(43) Seo, S. W.; Yang, J.-S.; Kim, I.; Yang, J.; Min, B. E.; Kim, S.; Jung, G. Y. Predictive Design of mRNA Translation Initiation Region to Control Prokaryotic Translation Efficiency. *Metab. Eng.* **2013**, *15*, 67−74.
(44) Mészáros, B.; Erdős, G.; Dosztányi, Z. IUPred2A: Context-Dependent Prediction of Protein Disorder as a Function of Redox State and Protein Binding. *Nucleic Acids Res.* **2018**, *46*, W329−W337.
(45) Wilbur, K. M.; Anderson, N. G. Electrometric and Colorimetric Determination of Carbonic Anhydrase. *J. Biol. Chem.* **1948**, *176*, 147−154.

https://dx.doi.org/10.1021/acs.biomac.0c00925
Biomacromolecules 2020, 21, 3847−3856

(46) Kalnciema, I.; Skrastina, D.; Ose, V.; Pumpens, P.; Zeltins, A. Potato Virus Y-Like Particles as a New Carrier for the Presentation of Foreign Protein Stretches. *Mol. Biotechnol.* **2012**, *52*, 129−139.
(47) Quenouille, J.; Vassilakos, N.; Moury, B. Potato Virus Y: a Major Crop Pathogen That Has Provided Major Insights into the Evolution of Viral Pathogenicity. *Mol. Plant Pathol.* **2013**, *14*, 439−452.
(48) Chen, X.; Zaro, J. L.; Shen, W.-C. Fusion Protein Linkers: Property, Design and Functionality. *Adv. Drug Deliv. Rev.* **2013**, *65*, 1357−1369.
(49) Mergulhão, F. J. M.; Summers, D. K.; Monteiro, G. A. Recombinant Protein Secretion in Escherichia coli. *Biotechnol. Adv.* **2005**, *23*, 177−202.
(50) Leith, E. M.; O'Dell, W. B.; Ke, N.; McClung, C.; Berkmen, M.; Bergonzo, C.; Brinson, R. G.; Kelman, Z. Characterization of the Internal Translation Initiation Region in Monoclonal Antibodies Expressed in Escherichia coli. *J. Biol. Chem.* **2019**, *294*, 18046−18056.
(51) Piatkov, K.; Vu, T.; Hwang, C.-S.; Varshavsky, A. Formyl-Methionine as a Degradation Signal at the N-Termini of Bacterial Proteins. *Microb. Cell* **2015**, *2*, 376−393.
(52) Donnelly, M. L. L.; Luke, G.; Mehrotra, A.; Li, X.; Hughes, L. E.; Gani, D.; Ryan, M. D. Analysis of the Aphthovirus 2A/2B Polyprotein 'Cleavage' Mechanism Indicates Not a Proteolytic Reaction, But a Novel Translational Effect: a Putative Ribosomal "Skip". *J. Gen. Virol.* **2001**, *82*, 1013−1025.
(53) Bonde, M. T.; Pedersen, M.; Klausen, M. S.; Jensen, S. I.; Wulff, T.; Harrison, S.; Nielsen, A. T.; Herrgaård, M. J.; Sommer, M. O. A. Predictable Tuning of Protein Expression in Bacteria. *Nat. Methods* **2016**, *13*, 233−236.
(54) Jagadish, M. N.; Huang, D.; Ward, C. W. Site-Directed Mutagenesis of a Potyvirus Coat Protein and Its Assembly in Escherichia coli. *J. Gen. Virol.* **1993**, *74*, 893−896.
(55) Malpica, C. A.; Voloudakis, A. E.; Aleman-Verdaguer, M. E.; Stark, D. M.; Fauquet, C. M.; Beachy, R. N. Structural Characterization of Tobacco Etch Virus Coat Protein Mutants. *Arch. Virol.* **2004**, *149*, 699−712.
(56) Hoarau, M.; Badieyan, S.; Marsh, E. N. G. Immobilized Enzymes: Understanding Enzyme - Surface Interactions at the Molecular Level. *Org. Biomol. Chem.* **2017**, *15*, 9539−9551.
(57) Saito, R.; Sato, T.; Ikai, A.; Tanaka, N. Structure of Bovine Carbonic Anhydrase II at 1.95 Å Resolution. *Acta Crystallogr. D Biol. Crystallogr.* **2004**, *60*, 792−795.
(58) Hang, H.; Bao, S.; Zhao, M.; Wang, B.; Zhou, S.; Jiang, B. Enzyme Membrane Reactor Coupled with Nanofiltration Membrane Process for Difructose Anhydride III from Inulin Conversion. *Chem. Eng. J.* **2015**, *276*, 75−82.
(59) Giorno, L.; Drioli, E. Biocatalytic Membrane Reactors: Applications and Perspectives. *Trends Biotechnol.* **2000**, *18*, 339−349.

https://dx.doi.org/10.1021/acs.biomac.0c00925
Biomacromolecules 2020, 21, 3847−3856